

Modeling clouds observed at SHEBA using a bulk microphysics parameterization implemented into a single-column model

H. Morrison

Program in Atmospheric and Oceanic Sciences, University of Colorado, Boulder, Colorado, USA

M. D. Shupe

Science and Technology Corporation, Boulder, Colorado, USA

J. A. Curry

School of Earth and Atmospheric Sciences, Georgia Institute of Technology, Atlanta, Georgia, USA

Received 24 February 2002; revised 15 August 2002; accepted 17 December 2002; published 30 April 2003.

[1] A single-column model coupled to a bulk microphysics parameterization (with prognostic cloud liquid water, cloud ice, rain, and snow mixing ratios) is evaluated using cloud properties retrieved at the Surface Heat Budget of the Arctic Ocean experiment (SHEBA) during the period of 1 April to 16 May 1998. Overall, the model accurately simulates the cloud boundaries and total cloud fraction, but has difficulty correctly partitioning the cloud phases and predicting the condensed water contents and paths. In particular, the mean liquid water path (LWP) is underestimated by 76%. This bias is attributed to underpredicting the liquid cloud fraction, that is, underpredicting the frequency of liquid- or mixed-phase clouds. The mean ice water path (IWP) is underestimated by 42%. Glaciation in the model occurs primarily through the preferential depositional growth of pristine ice initiated by deposition-condensation nucleation at the expense of liquid water, in contrast to glaciation mechanisms inferred from observations. Sensitivity tests are conducted to elucidate the relative importance of various microphysical parameters on the modeled cloud properties and processes. The liquid cloud fraction and mean LWP are most sensitive to uncertainties in the ice crystal number concentration, while the mean IWP is sensitive to several cloud ice/snow microphysical parameters, including the collection efficiency for riming and terminal fall velocities. The model evaluation is also discussed in the context of the spatial resolution and the approach to cloud scale separation. The unique spatial scales (particularly in the vertical) associated with Arctic stratiform clouds must be taken into account in order to correctly simulate the observed cloud properties. *INDEX TERMS:* 0320 Atmospheric Composition and Structure: Cloud physics and chemistry; 3309 Meteorology and Atmospheric Dynamics: Climatology (1620); 3349 Meteorology and Atmospheric Dynamics: Polar meteorology; *KEYWORDS:* Arctic, cloud, microphysics, mixed-phase, glaciation

Citation: Morrison, H., M. D. Shupe, and J. A. Curry, Modeling clouds observed at SHEBA using a bulk microphysics parameterization implemented into a single-column model, *J. Geophys. Res.*, 108(D8), 4255, doi:10.1029/2002JD002229, 2003.

1. Introduction

[2] The ability to accurately model cloud processes is of primary importance in correctly simulating the Arctic climate system. Cloud parameterizations used in global and regional models have typically been developed for lower latitude regions. Thus, these models are often deficient in simulating Arctic cloudiness [e.g., Curry *et al.*, 1996]. Modeling difficulties arise from several unique cloud properties [Curry *et al.*, 1996]: complex vertical structure with multiple layers, wintertime ice crystal plumes associated with leads, “clear-sky” ice crystal precipitation, and persis-

tent mixed-phase clouds. Biases in the modeled bulk and microphysical cloud properties may lead to errors in the surface radiative fluxes and hence uncertainties in the surface energy balance [Curry and Ebert, 1990; Curry *et al.*, 1993]. There is particular interest in improving simulations of Arctic climate because of the importance of Arctic climate processes to global climate feedbacks [Curry *et al.*, 1996]. This interest motivated the Surface Heat Budget of the Arctic Ocean experiment [SHEBA; Uttal *et al.*, 2002], which provided a comprehensive data set for evaluating model parameterizations.

[3] A common method for testing parameterizations is through a single-column model (SCM), taken to represent a single grid cell in a 3-D model [e.g., Randall *et al.*, 1996]. Large-scale dynamics and advection in a SCM are specified

through observational or model analysis [Randall and Cripe, 1999]. Single-column modeling allows for a first-order evaluation of parameterizations without added complications due to feedbacks with the large-scale dynamics. Preliminary studies have indicated significant biases associated with SCM simulations of clouds observed at SHEBA [Curry *et al.*, 2000]; the need for a better understanding and quantification of these biases has motivated the research presented here. In this study, a version of the *Dudhia* [1989] bulk cloud microphysics parameterization, modified to simulate mixed-phase clouds in the Fifth-Generation Penn State/NCAR Mesoscale Model (MM5; NCAR technical note by G. A. Grell *et al.*, available at <http://www.mmm.ucar.edu/mm5/doc.html>, 1995) and the Arctic Regional Climate System Model (ARCSyM; Lynch *et al.*, 1995), is implemented into a SCM to simulate the 1 April to 16 May 1998 period of SHEBA (hereafter this microphysics parameterization is referred to as the “MM5mp”).

[4] There are different approaches to testing parameterizations in a SCM, depending upon the level of constraint specified in the model, as described by Randall *et al.* [1996]. In a more prognostic approach, the thermodynamic profiles are predicted using tendencies calculated for all of the parameterized physical processes (in addition to the tendencies specified by the forcing). In a more diagnostic approach, tendencies due to one or more parameterized processes are specified. The diagnostic strategy would be less useful for the case presented here because the observed tendencies are not well characterized. In addition, feedbacks between the clouds, turbulence, radiative transfer, and atmospheric stability, which may be the primary modulator of low-level Arctic clouds [Curry, 1986], would be neglected to some degree, depending upon the level of constraint. Therefore, we evaluate the SCM in a more prognostic context, keeping in mind that the results reflect interactions between all of the modeled physical processes, as well as the forcing and initial conditions. Although this approach does not allow us to identify any specific sources of error, it does allow a general evaluation of the modeled clouds, and, in the context of sensitivity tests, gives an idea of the relative importance of uncertainties associated with the various microphysical parameters. In this way, a more general picture of the microphysical parameterization emerges, which may then be clarified through higher resolution, shorter duration case studies and incorporation into 3-D models.

[5] The goal of this study is to determine the effectiveness of a SCM that employs the MM5mp parameterization in simulating clouds observed at SHEBA during the springtime transition season. In addition, we investigate the model sensitivity to a number of specified microphysical parameters and discuss issues associated with modeling Arctic clouds in the context of the general SCM structure (i.e., the model resolution and approach to cloud scale separation).

2. Model Description

[6] A new single-column model (ARCSCM) has been developed for evaluating parameterizations and studying thermodynamic processes and feedbacks in the Arctic. Prognostic variables include temperature and water vapor, cloud liquid water, cloud ice, snow, and rain mixing ratios. ARCSCM has a sigma coordinate system; thirty vertical

levels with increasing resolution toward the surface are used here. The horizontal domain, effectively given by the scale of the dynamic forcing, is approximately 60×60 km. Surface boundary conditions, horizontal wind, vertical pressure velocity, and total (3-D) advection of temperature (including adiabatic compression/expansion) and water vapor mixing ratio are specified. The time tendencies of temperature, T , and water vapor mixing ratio, q_v , at each level are given by the following equations:

$$\frac{\partial T}{\partial t} = -\nabla \cdot \vec{v}T - \left(\frac{\partial}{\partial p} - \frac{R_d}{c_p p} \right) \omega T + \left(\frac{\partial T}{\partial t} \right)_{\text{RAD}} + \left(\frac{\partial T}{\partial t} \right)_{\text{TUR}} + \left(\frac{\partial T}{\partial t} \right)_{\text{MIC}} + \left(\frac{\partial T}{\partial t} \right)_{\text{CON}}, \quad (1)$$

$$\frac{\partial q_v}{\partial t} = -\nabla \cdot \vec{v}q_v - \frac{\partial}{\partial t} \omega q_v + \left(\frac{\partial q_v}{\partial t} \right)_{\text{TUR}} + \left(\frac{\partial q_v}{\partial t} \right)_{\text{MIC}} + \left(\frac{\partial q_v}{\partial t} \right)_{\text{CON}}, \quad (2)$$

where \vec{v} is the horizontal wind vector, ω is the vertical pressure velocity, p is the pressure, R_d is the gas constant for air, c_p is the specific heat of air at constant pressure, RAD is the radiative heating rate, TUR is the turbulent diffusion tendency, MIC is the cloud microphysical tendency, and CON is the convective tendency.

[7] Shortwave radiative transfer is treated using the two-stream delta-eddington method with 18 spectral intervals between $0.2 \mu\text{m}$ and $5 \mu\text{m}$, following Breigleb [1992]. The parameterization of cloud optical properties follows from Slingo [1989] for cloud droplets and Ebert and Curry [1992] for cloud ice. The cloud particle effective radius, r_e , is specified to be $10 \mu\text{m}$ for liquid droplets and $40 \mu\text{m}$ for ice. Longwave radiative transfer is given by the Rapid Radiative Transfer Model (RRTM; Mlawer *et al.*, 1997), using 16 spectral intervals between 5 and $500 \mu\text{m}$. The effects of precipitation-size particles on radiative transfer are ignored. Surface emissivity is prescribed at 0.99.

[8] The boundary layer parameterization is a first-order nonlocal scheme following Holtslag and Boville [1993]. Turbulent diffusion is calculated for temperature, water vapor, cloud liquid water, and cloud ice. Sensible and latent surface turbulent fluxes are calculated following Schramm *et al.* [1997]. The effects of leads on the surface fluxes are ignored.

[9] Following the convention of many mesoscale models (e.g., MM5, ARCSyM, and others), cloud and precipitation physics is divided into two categories based upon the separation between large-scale (resolvable) and subgrid scale processes [the “full-physics” set-up as described by Zhang *et al.*, 1988]. Large-scale cloud and precipitation processes are explicitly determined with the bulk microphysics parameterization coupled to the grid-box-averaged thermodynamic properties, while subgrid scale processes are implicitly treated with the modified Arakawa-Schubert convective parameterization of Grell [1993]. Even though the large-scale microphysics scheme may explicitly resolve the largest convective elements of cloud systems depending upon the model resolution [Zhang *et al.*, 1988], given that deep convection is essentially absent in the multiyear ice zone of the Arctic basin (which includes the SHEBA site),

we assume that the resolved clouds are stratiform in type, and will refer to them as such for the remainder of the paper. The subgrid convective parameterization does not explicitly calculate cloud water contents, but does feedback to the full column through vertical distributions of heating and moistening and the removal of water vapor through precipitation. Some large-scale models [e.g., *Ose, 1993; Fowler et al., 1996*] explicitly couple the subgrid and resolvable cloud parameterizations by adding detrained condensed water to the prognostic water of the large-scale cloud scheme. However, since deep convection is very limited in the region, we assume that excluding convective cloud water in the model will have little effect on the overall results. Implications of this approach to cloud scale separation are discussed in section 6.

[10] The microphysics scheme is a version of the MM5mp bulk mixed-phase parameterization currently implemented in MM5 and ARCSyM. Four prognostic condensed water variables are included in the parameterization: cloud liquid water (q_c), cloud ice (q_i), rain (q_r), and snow (q_s) mixing ratios. The time tendencies of these variables are given by the following equations:

$$\frac{\partial q_c}{\partial t} = -\frac{\partial}{\partial p}(\omega q_c) + \delta_c + \text{PCC} + \text{MLTIC} - \text{PRC} - \text{PRA} - \text{NUFCI} - \text{HOFCI} - \text{PSACW}, \quad (3)$$

$$\frac{\partial q_i}{\partial t} = -\frac{\partial}{\partial p}(\omega q_i) + \frac{\partial}{\partial \sigma} \left(\frac{\bar{V} \rho g q_i}{p_s - p_{\text{top}}} \right) + \delta_i + \text{PRD} + \text{PRI} - \text{MLTIC} + \text{NUFCI} + \text{HOFCI} - \text{PRCI} - \text{PRAI}, \quad (4)$$

$$\frac{\partial q_r}{\partial t} = -\frac{\partial}{\partial p}(\omega q_r) + \frac{\partial}{\partial \sigma} \left(\frac{\bar{V} \rho g q_r}{p_s - p_{\text{top}}} \right) + \text{PRE} + \text{PSMLT} + \text{PRA} + \text{PRC} - \text{NUFCIR}, \quad (5)$$

$$\frac{\partial q_s}{\partial t} = -\frac{\partial}{\partial p}(\omega q_s) + \frac{\partial}{\partial \sigma} \left(\frac{\bar{V} \rho g q_s}{p_s - p_{\text{top}}} \right) + \text{PREI} + \text{PRAI} + \text{PRCI} - \text{PSMLT} + \text{PSACW} + \text{NUFCIR}, \quad (6)$$

where p_s is the air pressure at the surface, p_{top} is the air pressure at the top of the model (50 mb), \bar{V} is the mass-weighted mean particle terminal fall velocity, g is the acceleration due to gravity, σ is the model sigma level, ρ is the air density, δ_c and δ_i are the turbulent flux divergence for cloud liquid water and cloud ice, respectively, and the microphysical processes (e.g., PCC, PRC, PRA, etc.) are given in Table 1. In addition, the latent heating rate $\left(\frac{\partial T}{\partial t}\right)_{\text{MIC}}$ and cloud microphysical water vapor mixing ratio tendency $\left(\frac{\partial q_v}{\partial t}\right)_{\text{MIC}}$ are given by:

$$\begin{aligned} \left(\frac{\partial T}{\partial t}\right)_{\text{MIC}} &= \frac{L_v}{c_p}(\text{PCC} + \text{PRE}) + \frac{L_s}{c_p}(\text{PRI} + \text{PREI} + \text{PRD}) \\ &+ \frac{L_f}{c_p}(\text{NUFCI} + \text{HOFCI} + \text{PSACW} - \text{MLTIC} \\ &- \text{PSMLT} + \text{NUFCIR}), \end{aligned} \quad (7)$$

Table 1. Summary of Microphysical Processes in the MM5mp Parameterization

	Description
HOFCI	Homogeneous freezing of cloud water
MLTIC	Melting of cloud ice
NUFCI	Heterogeneous freezing of cloud water
NUFCIR	Freezing of rain
PCC	Condensation/evaporation of cloud water
PRA	Accretion of cloud water by rain
PRAI	Accretion of cloud ice by snow
PRC	Autoconversion of cloud water to rain
PRCI	Autoconversion of cloud ice to snow
PRD	Deposition/sublimation of cloud ice
PRE	Condensation/evaporation of rain
PREI	Deposition/sublimation of snow
PRI	Initiation of cloud ice
PSACW	Riming of cloud water
PSMLT	Melting of snow

$$\left(\frac{\partial q_v}{\partial t}\right)_{\text{MIC}} = -\text{PCC} - \text{PRI} - \text{PRD} - \text{PRE} - \text{PREI}, \quad (8)$$

where L_v , L_s , and L_f are the latent heats of vaporization, sublimation, and fusion, respectively. A box diagram (Figure 1) shows the relationship between the various condensed water species and the microphysical processes that transit water between them.

[11] Because of the difficulty in specifying appropriate horizontal advective tendencies of the condensed water species, these terms are neglected. Vertical advection of condensed water is calculated using the specified vertical pressure velocities and the modeled condensed water profiles. Entrainment and fallout of cloud droplets is neglected. Fractional cloudiness within the column is not considered; instantaneous cloud fraction is 1 if any model level has a condensed water content greater than the threshold value of 10^{-5} g m^{-3} , and 0 otherwise, following ARCSyM. Formulations for the various microphysical processes are given in Appendix A.

3. Data

[12] The SHEBA field project, conducted from October 1997 to October 1998, provided a comprehensive source of data to force and evaluate climate models. SHEBA was coordinated with the FIRE [First ISCCP (International Satellite Cloud Climatology Project) Regional Experiment] Arctic Clouds Experiment [*Curry et al., 2000*] and the Atmospheric Radiation Measurement (ARM) program [*Stokes and Schwartz, 1994*]. The SHEBA field program consisted of a heavily instrumented icebreaker ship (the Canadian Coast Guard Des Groseilliers) frozen into the sea ice on 1 October 1997, at 75.16° N , 142.41° W . The station drifted with the ice for one year across the Beaufort and Chukchi Seas, with measurements focused on surface energy balance and sea ice mass balance. ARM provided several surface-based instruments to measure clouds and radiation, while FIRE-ACE used research aircraft to provide in-situ and remote measurements of atmospheric and surface characteristics.

[13] Temperature and relative humidity profiles were measured by rawinsondes launched from the ice station

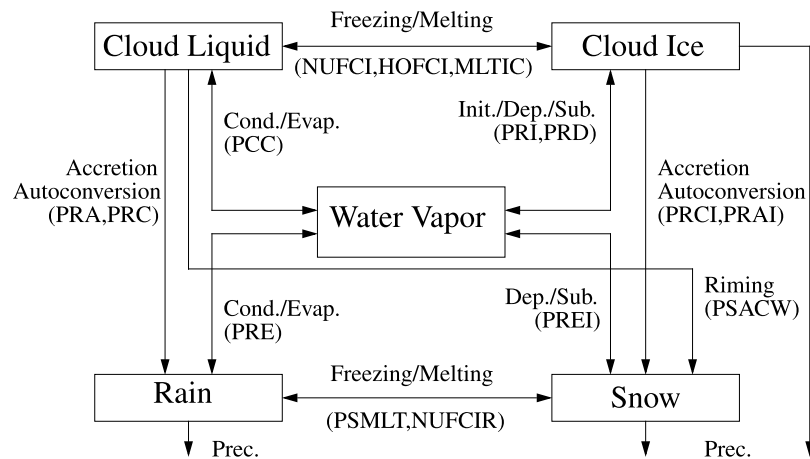


Figure 1. Box diagram illustrating the cloud microphysics parameterization. The microphysical processes are given in Table 1.

two to four times per day during the period of interest. A Nipher shielded snow gauge system measured total accumulations of precipitation on a daily basis (or as new precipitation warranted). The precipitation data were corrected by the SHEBA Project Office to take into account various factors of the high-latitude environment (e.g., blowing snow).

[14] Cloud properties were determined from a collection of ground-based measurements at the SHEBA ice camp. A vertically pointing, 35-GHz, millimeter cloud radar (MMCR) made continuous measurements of radar reflectivity and Doppler velocity up to a height of 13 km over the ice station. Radar data were averaged over 1-minute time periods. Collocated with the radar were a microwave radiometer (MWR) that measured brightness temperatures at 23.8 and 31.4 GHz, and a dual-polarization lidar. These instruments are used to determine the cloud fraction, vertical layering, and microphysical properties.

[15] Retrieval techniques for estimating the cloud microphysical parameters are discussed in detail in *Shupe et al.* [2001], and are briefly summarized here. All clouds observed by the MMCR are classified as all-ice, all-liquid, mixed-phase, snow, rain, or drizzle. The classifications are based on radar measurements, lidar depolarization ratios, MWR brightness temperature measurements, temperature and relative humidity soundings, and surface observer codes. The appropriate retrieval method is then applied to each cloud based upon its classification.

[16] Ice water content (IWC), mean particle size, and ice particle concentration are retrieved using three complementary techniques. Empirical relationships of the form $IWC = a_1 Z^{b_1}$ are used to relate ice cloud parameters directly to radar reflectivity, Z . Mean values of the a_1 and b_1 coefficients for the SHEBA region during the period of interest are used. Additionally, the *Matrosov* [1999] technique, which uses measurements of IR sky brightness temperature to effectively tune the a_1 coefficient to a given cloud scene, is employed. Third, the *Matrosov et al.* [2002] technique is applied, where a relationship between radar Doppler fall velocity and particle size is used for retrieving the cloud parameters. Since the radar signal is proportional to particle size to the sixth power, we assume that the ice

particles dominate the radar signal from mixed-phase clouds. Therefore, the radar-only techniques (simple empirical and *Matrosov et al.* [2002]) are used to retrieve the ice component of mixed-phase clouds. Retrievals for the snow microphysical parameters (IWC, mean particle size, number concentration) are based on the particle size distributions of *Gunn and Marshall* [1958]. Application of these techniques to mixed-phase clouds is of unknown certainty, but is currently the most reasonable method for retrieving the ice component from these clouds. For cloud ice and snow, ice water path (IWP) is calculated by vertically integrating the IWC profiles. Total column-integrated liquid water path (LWP) and precipitable water vapor (PWV) are retrieved from MWR measurements of brightness temperature according to the method described by *Westwater et al.* [2001].

[17] Cloud boundaries are based on combined radar-lidar data [*Intrieri et al.*, 2002]. In general, the lidar is used to determine the cloud base, since the radar responds to precipitation as well as cloud water. The cloud top is typically determined by radar, since the lidar is often attenuated at a lower level in the cloud. Because the radar may not detect small particles near the cloud top, its height may be underestimated [*Intrieri et al.*, 2002]. Various cloud fractions (separated by type and altitude) are based on radar measurements and cloud type classifications.

[18] All water contents and paths presented here are combinations of cloud water and precipitation. However, liquid-phase precipitation during this time period was negligible. Hereafter, “LWP” will refer to the combined cloud liquid and rainwater paths, “IWP” to the combined cloud ice and snow water paths, and “IWC” to the combined cloud ice and snow water contents, for both the modeled and retrieved values. In addition, “liquid cloud fraction” will refer to the fraction of time that cloud liquid water or rain is present in the column, and “ice cloud fraction” will refer to the fraction of time that cloud ice or snow is present in the column. Therefore, mixed-phase clouds contribute to both the liquid cloud fraction and the ice cloud fraction, so that the sum of these fractions may exceed 100%. “Total cloud fraction” is the fraction of time that liquid and/or ice is present. Cloud presence is

defined in the model by a water content threshold value of 10^{-5} g m^{-3} .

[19] In this study, retrieved values are used as a ground truth to compare with the model results. Instantaneous retrieval uncertainties for various parameters may be significant. *Matrosov et al.* [2002] showed relative standard deviations of $\sim 55\%$ between IWC retrievals and in situ measurements made during late April near SHEBA. Instrument noise and retrieval uncertainties contribute to an instantaneous uncertainty of approximately 25 g m^{-2} in the LWP retrievals [*Westwater et al.*, 2001]. However, since the retrieval methods were developed using statistically derived relationships, uncertainties in the statistical values of the retrieved cloud properties presented here are expected to be much smaller than uncertainties in the instantaneous values. We infer this from an analysis of the clear-sky LWP retrievals that reveals a Gaussian-type distribution centered at -4 g m^{-2} . Since factors contributing to uncertainty in the clear-sky retrievals (e.g., instrument noise, uncertainties in atmospheric profiles, uncertainties in absorption coefficients, etc.) also contribute to uncertainty in the cloudy-sky retrievals, the small bias in the mean of the clear-sky LWP retrievals suggests that the bias in the mean cloudy-sky retrievals is small as well (although this does not rule out a systematic error in the cloudy-sky retrievals due to uncertainty in the liquid water absorption coefficients). A similar analysis is not possible for the retrieved IWP, since this is determined from reflectivity measurements (no reflectivity in clear sky by definition) rather than atmospheric brightness temperatures. Thus uncertainties in the ice properties averaged over the time period are not as well characterized.

4. Baseline Simulation Results

[20] The 1 April-16 May 1998 period of SHEBA is simulated using ARCSM. Initial and boundary conditions are given by European Centre for Medium-Range Weather Forecasts (ECMWF) model output and SHEBA observations. Hourly values of the total (3-D) temperature and water vapor mixing ratio advection (including adiabatic temperature tendency), horizontal wind, and vertical pressure velocity for the grid cell overlying the SHEBA site were obtained from 12 to 35 hour forecasts of the ECMWF model (version 13R4). The ECMWF data has 31 vertical levels and nominal 60 km grid spacing, and was recently improved by the ECMWF to produce the equivalent of a “reanalysis.” A correction factor is also applied at each

Table 2. Comparison of Modeled and Observed Cloud Bottom Height (Lowest Layer), Cloud Top Height (Top Layer), Layer Thickness, and Number of Layers

	Cloud Bottom (Lowest Layer), m	Cloud Top (Top Layer), m	Layer Thickness, m	Number of Layers
Modeled Mean	330	4344	2010	1.51
Observed Mean	399	3824	1924	1.35
Model Standard Deviation	958	2600	1963	0.65
Observed Standard Deviation	1080	2719	1746	0.59

Table 3. Comparison of Modeled and Observed Cloud Fractions^a

	Liquid Fraction	Ice Fraction	Total Fraction
Modeled	12.0	76.0	76.0
Observed	64.4	74.8	85.4

^aValues are given in percent.

level to the ECMWF temperature and water vapor mixing ratio advections, following H. Morrison and J. O. Pinto (A new approach for obtaining advection profiles: Application to SHEBA single-column modeling studies, submitted to *Monthly Weather Review*, 2003) (hereinafter referred to as Morrison and Pinto, submitted manuscript, 2003). Although this correction factor constrains the time-averaged column-integrated temperature and water vapor advections to the observed budgets, there is still uncertainty associated with their vertical and temporal distributions. These forcing data are linearly interpolated to ARCSM levels. Hourly surface temperature, pressure, and albedo are obtained from SHEBA tower measurements [*Persson et al.*, 2002], while the surface water vapor mixing ratio is given by saturation with respect to ice ($<0^\circ\text{C}$) or liquid water ($>0^\circ\text{C}$). All hourly forcing data are linearly interpolated to the model time step of 1 minute. Simulations are initialized using T and q_v profiles derived from a combination of rawinsonde, tower, and ECMWF model data. Below 50 m, where the rawinsonde is prone to error, profiles of T and q_v are obtained by linearly interpolating between 10 m tower data and 50 m sonde data. ECMWF model data is used above the maximum height of the sonde ($\sim 19 \text{ km}$).

[21] The model evaluation is broadly divided into two parts. First, we compare the statistics of several modeled and observed/retrieved cloud properties, including vertical distribution, fraction, IWP, LWP, and IWC. Second, we examine budgets of the simulated cloud water and supersaturation and conduct sensitivity tests of the model microphysical parameters. Because of the statistical nature of the retrievals, the difference in scale between the model and the observations (see section 6), and the reduced bias in the ECMWF advective forcing when the data are averaged over longer time periods (Morrison and Pinto, submitted manuscript, 2003), the analysis in this paper focuses on statistics of the cloud properties calculated for the entire period (rather than instantaneous values).

[22] Overall, the modeled cloud heights are fairly well-predicted, although the mean modeled height of the highest cloud top is higher than observed, and the model produces somewhat thicker and more numerous cloud layers (Table 2). It should be noted, however, that the observed cloud top height may be biased low (see section 3).

[23] In general, the model has difficulty correctly partitioning cloud phase and tends to underpredict the condensed water paths (see Tables 3 and 4). The mean modeled LWP is significantly underestimated, while the modeled LWP_{n0} (mean mixed- and liquid-phase in-cloud LWP) is larger than the retrieved value. These biases are consistent with the substantial underprediction of liquid cloud fraction. Mean values of the simulated IWP and IWP_{n0} (mean mixed- and ice-phase in-cloud IWP) are smaller than the retrieved values. The modeled ice cloud fraction and total cloud fraction are fairly close to the observed values. We note that the modeled cloud fractions (liquid, ice, and total) are

Table 4. Comparison of Modeled and Retrieved LWP, IWP, LWP_{n0}, and IWP_{n0}^a

	LWP	IWP	LWP _{n0}	IWP _{n0}
Modeled Mean	6.1	20.2	51.6	26.5
Retrieved Mean	25.6	34.6	36.2	41.1
Modeled Standard Deviation	19.6	52.3	29.8	58.5
Retrieved Standard Deviation	45.4	92.1	53.9	100.3

^aValues are given in g m^{-2} .

insensitive to the cloud fraction threshold value over the range of 10^{-3} to 10^{-7} g m^{-3} . Standard deviations of the modeled water paths are about half as large as the retrieved values, which may reflect variability in the observed cloud field that is not captured by the grid-box-averaged cloud properties produced by the model (see section 6).

[24] The temporal distributions of simulated and retrieved LWP clearly illustrate the large biases in mean LWP and liquid cloud fraction (Figure 2). The retrievals show intermittent liquid water throughout the study period, with the exception of 21–25 April, while the model predicts only three liquid water events: 29 April, 8–9 May, and 11–15 May. When liquid water is present in the simulation, however, the LWP is quite large; this feature is consistent with the relatively large modeled values of LWP_{n0} compared to the retrievals.

[25] The model biases are primarily associated with low-level (<3 km), rather than high-level (>3 km) clouds. Modeled means and standard deviations of the IWP and IWP_{n0} above 3 km are close to retrieved values. In contrast, these values are underpredicted below 3 km (Tables 5 and 6). Liquid water predominately occurs below 3 km in both the observations and model. The ice cloud fraction is somewhat overpredicted for both high- and low-level cloudiness. The distribution of bias with height may be interpreted in the context of driving mechanisms for the formation and occurrence of clouds over the Arctic region. Mid and upper-level clouds in the Arctic are believed to be associated with frontal systems [Curry and Herman, 1985],

Table 5. Comparison of Modeled and Retrieved IWP and IWP_{n0} for Low and High Clouds^a

	Low Cloud IWP	<3 km IWP _{n0}	High Cloud IWP	>3 km IWP _{n0}
Modeled Mean	15.8	21.5	4.4	8.0
Retrieved Mean	30.4	37.1	4.3	9.7
Modeled Standard Deviation	39.2	44.4	14.5	18.9
Retrieved Standard Deviation	86.4	95.5	16.0	23.9

^aValues are given in g m^{-2} .

while low-level clouds are less sensitive to the synoptic-scale situation and instead tend to form as a result of air-mass modification over the polar basin [Curry, 1983]. Therefore, the fairly well-predicted upper-level cloudiness in the model suggests that the synoptic-scale forcing is adequate. On the other hand, the poor simulation of lower-level cloudiness indicates deficiencies associated with the model physics.

[26] Biases associated with the modeled IWC are consistent with biases in the IWP and IWP_{n0} (see Table 7), since the cloud thickness and ice cloud fraction are generally well-predicted. The modeled values of mean IWC for all clouds and clouds below 3 km are significantly smaller than the retrieved values. In contrast, the modeled values of mean IWC for mixed-phase clouds and high clouds (>3 km) are similar to the retrieved values. Standard deviations of the modeled IWC are generally much smaller than the retrieved values.

[27] Probability density functions (PDFs) of the simulated and retrieved LWP demonstrate the much smaller mean and variance of the modeled LWP (Figure 3a). An interesting feature is the difference in shape between the modeled and retrieved PDFs: the retrieved PDF shows a nearly asymptotic rise toward lower values of LWP, while the modeled PDF doesn't have any clear trend between LWP values of 1 and 100 g m^{-2} . This difference in shape may be due in part

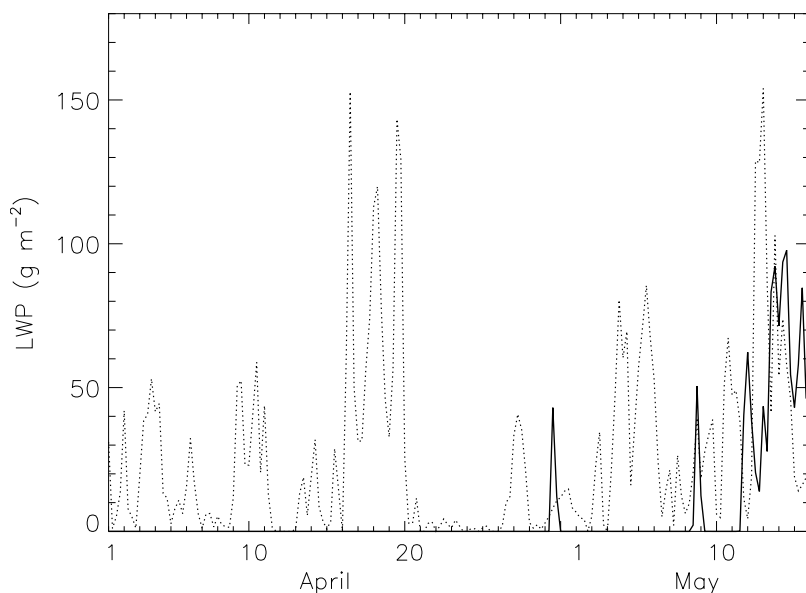
**Figure 2.** Modeled (solid) and retrieved (dotted) timeseries of LWP (data are 6-hour averages).

Table 6. Comparison of High and Low Cloud Fractions^a

	Low Cloud Liquid Fraction	<3 km Ice Fraction	High Cloud Liquid Fraction	>3 km Ice Fraction
Modeled	12.0	73.6	0.0	54.3
Observed	63.7	68.9	8.5	44.1

^aValues are given in percent.

to horizontal variability in the cloud field that is not captured in the grid-box averaged quantities produced by the model. *Considine et al.* [1997] show bimodal LWP PDFs for homogeneous layered clouds (when clear-sky values are included), but in clouds with greater horizontal variability, the PDFs instead rise asymptotically toward lower values of LWP. The large difference between the modeled and retrieved PDFs at LWP values less than 25 g m⁻² may also be due to retrieval noise in clear-sky conditions. Retrieval noise may be responsible for the relative smoothness of the retrieved PDF in comparison with the model.

[28] In general, the modeled IWP PDF is consistent with the retrieved IWP PDF (Figure 3b). The primary difference is the reduced variance in the modeled PDF, so that probability densities in the model PDF are generally larger than the retrieved values at IWP values less than ~70 g m⁻², while they are generally smaller above ~70 g m⁻². The relative smoothness of the retrieved IWP PDF compared with the modeled PDF may be due to retrieval noise.

[29] Biases associated with the low-level clouds are further illustrated by plots of modeled and retrieved values of LWP/TWP (TWP refers to the total condensed water path) versus cloud-top temperature for clouds below 3 km (Figure 4). Figure 4 shows modeled values of LWP/TWP larger than 0.5 at temperatures warmer than 260 K, while ice-phase clouds (LWP/TWP equal to zero) are present up to 268 K. Values of the retrieved LWP/TWP near 1 occur at temperatures below 250 K. There are no ice-phase clouds at temperatures warmer than 260 K in the retrievals. It is noted that LWP retrieval noise will lead to uncertainty in the LWP/TWP values, which could result in ice-phase clouds having a retrieved LWP/TWP ratio greater than zero. However, most of the observed clouds with tops below 3 km contained at least some liquid. Thus the model tends to overpredict the amount of cloud ice relative to liquid, particularly at temperatures below 260 K. This analysis may partially explain why the model more accurately predicts the LWP at the end of the simulation (see Figure 2), when low-level temperatures are generally warmer than earlier in the period.

[30] Although the model underpredicts the mean condensed water paths, particularly for liquid, an analysis of the bulk (column-integrated) water budget indicates an overall excess of water in the model. The bulk water budget may be expressed as (Morrison and Pinto, submitted manuscript, 2003):

$$\frac{\Delta\text{PWV}}{\delta t} = \text{ADV} + \text{MF} - \frac{\text{PREC}}{\delta t}, \quad (9)$$

where δt is the length of the time period, ΔPWV is the change in precipitable water vapor, ADV is the time-

averaged vertically integrated water vapor advection, MF is the time-averaged surface mass flux of water vapor (i.e., surface sublimation/deposition), and PREC is the total precipitation reaching the surface during the time period. The change in condensed water path has been excluded for simplicity; it accounts for only ~1% of the total water budget in both the model and observations. Observed and modeled values for the terms in equation (9) are given in Table 8. The time-averaged vertically integrated advective forcing in the model is constrained to the observed budget through a correction algorithm described by Morrison and Pinto (submitted manuscript, 2003); the small difference in this term between the modeled and observed budgets results from interpolating to the ARCSM model levels. The modeled precipitation flux (predominately cloud ice/snow) is slightly larger than observed. Convection accounts for approximately 3% of the total modeled precipitation. Most of the excess water in the modeled budget is attributed to the surface water vapor flux, which is opposite in sign to the observations. On average, the model sublimates water from the surface, while the observations show a small deposition.

[31] The mean modeled temperature and water vapor mixing ratio profiles are somewhat warmer and more moist than observed (Figure 5a and 5b). The modeled water vapor mixing ratio profile shows a moist plume at 900 mb. This feature may be associated with an unrealistic turbulent transport of water vapor that results in a net moisture flux from the surface to just above the boundary layer, which is consistent with the excess surface water vapor flux in the simulation. In contrast, the mean modeled relative humidity profile (Figure 5c) shows an overall dry bias, particularly below 900 mb, that is associated with the underprediction of the mean IWP and LWP in the lower-level clouds. The overprediction of precipitation (see Table 8), coincident with the underpredicted relative humidity, suggests that excessive precipitation drying may be partially responsible for this low-level relative humidity bias.

5. Budget Analysis of the Cloud Liquid Water and Supersaturation

[32] The results from section 4 show that the modeled liquid cloud fraction is substantially underestimated. Because cloud liquid water is the main contributor to the modeled LWP (the rainwater path is much smaller), we analyze the cloud water budget during liquid water formation and dissipation to investigate this bias. Initiation of cloud liquid water is determined by the condensation rate ($\text{PCC} > 0$), because condensation represents the only significant source term for cloud liquid water in the model

Table 7. Comparison of Modeled and Retrieved IWC^a

	IWC (Total)	IWC (Mixed-Phase)	IWC (<3 km)	IWC (>3 km)
Modeled Mean	0.0111	0.0127	0.0128	0.0040
Retrieved Mean	0.0243	0.0165	0.0453	0.0051
Modeled Standard Deviation	0.0178	0.0070	0.0190	0.0088
Retrieved Standard Deviation	0.2050	0.0474	0.2950	0.0114

^aValues are given in g m⁻³.

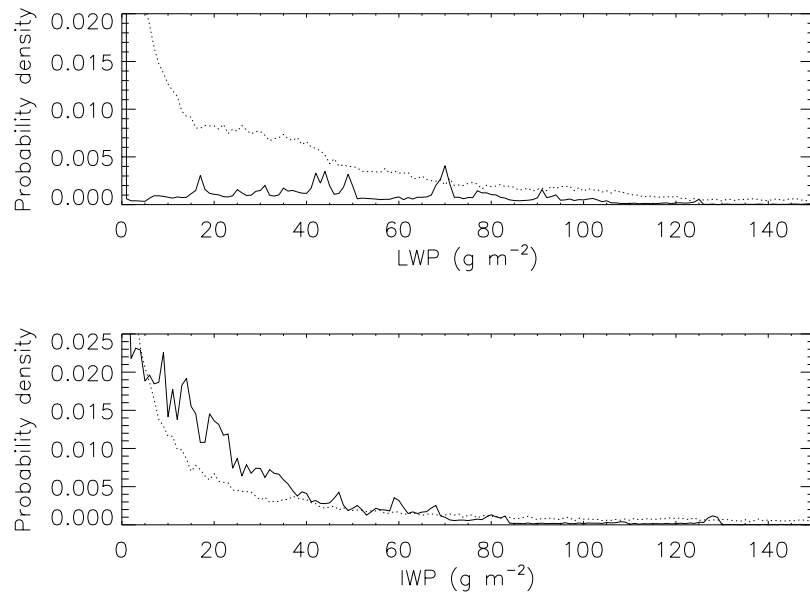


Figure 3. Modeled (solid) and retrieved (dotted) probability density functions for (a) liquid and (b) ice water paths.

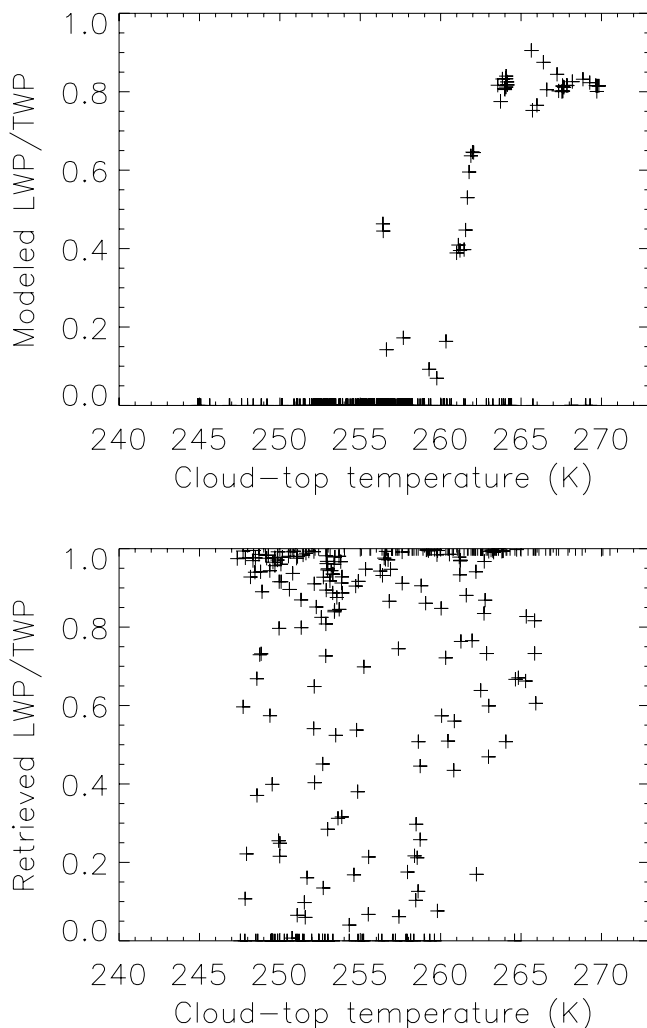


Figure 4. (a) Modeled and (b) retrieved values of LWP/TWP versus cloud top temperature, for all clouds below 3 km.

(melting of cloud ice is negligible and advection of liquid water into the column has been excluded).

[33] Dissipation of cloud liquid water is more complicated because there are multiple sink terms (PCC < 0, PSACW, PRA, PRC, NUFCl, HOFCl). In the 10-minute period prior to the complete dissipation of cloud liquid water (defined as the reduction of liquid water content below the threshold of 10^{-5} g m^{-3}), the mean value of PCC is ~ 30 times larger than the next largest sink term, PSACW. This result is consistent with the formulations for the various microphysical processes in the parameterization (see Appendix A); PCC is the only term in the cloud liquid water budget that is not a function of q_c , so that evaporation rates may remain large even as q_c becomes small (to the point of complete dissipation). Thus PCC is the primary term directly influencing the duration of the modeled liquid water.

[34] PCC is a function of the psychrometric correction factor (r_1 in equation (A20)), and the absolute supersaturation, δM , where $\delta M = q_v - q_{vs}$. Other modelers have discussed the role of the saturation relaxation timescale on the condensation rate [e.g., *Khvorostyanov and Curry, 1999*]. Here, condensation/evaporation is assumed to be an instantaneous process; the saturation relaxation timescale is therefore effectively equal to the model time step.

[35] Processes controlling the evolution of δM are examined to elucidate uncertainties in PCC during cloud liquid water formation and dissipation. Four parameterized processes within the model affect the evolution of temperature

Table 8. Comparison of the Modeled and Observed Bulk Water Budgets^a

	$\frac{\Delta PWV}{\Delta t}$	ADV	MF	$\frac{PREC}{\Delta t}$
Modeled	0.00176	0.00676	0.000594	0.00565
Observed	0.00102	0.00647	-0.00002	0.00543

^aValues are given in $\text{g m}^{-2} \text{ s}^{-1}$.

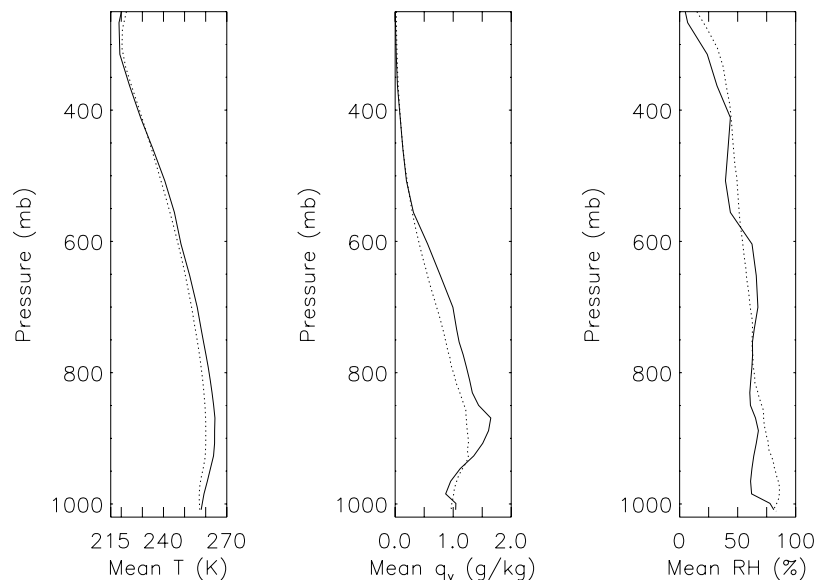


Figure 5. Mean modeled (solid) and observed (dotted) temperature, (a) T , (b) water vapor mixing ratio, q_v , and (c) relative humidity, RH profiles.

and water vapor mixing ratio and thus the supersaturation: (1) cloud microphysical processes, (2) radiative transfer, (3) T and q_v advection and adiabatic expansion (hereafter referred to as “advection”), and (4) turbulent mixing. The relative contributions of these processes to the formation and dissipation of cloud liquid water (Table 9) are determined by calculating the mean supersaturation tendencies during the 10-minute period prior to the increase of $PCC > 0$ (condensation), and during the 10-minute period after the reduction of $PCC < 0$ (evaporation). Advection is the primary source for supersaturation prior to condensation, while turbulence and radiative cooling are secondary production terms. It is evident that the cloud microphysics tendency initiates evaporation, since advection, radiative transfer, and turbulence remain sources for supersaturation after the onset of evaporation. Deposition of water vapor onto cloud ice (PRD) and snow (PREI) dominates the cloud microphysical supersaturation tendency. During the lifetime of the mixed-phase cloud, the ice particle growth rate increases due to the positive feedback between the cloud ice/snow mixing ratios and the rate of depositional growth. Eventually, the deposition rate becomes too large to balance the source terms for supersaturation, the relative humidity decreases, and the cloud drops begin to evaporate. Thus, the Bergeron-Findeisen mechanism (i.e., preferential depositional growth of ice over liquid due to the lower saturation vapor pressure) is mostly responsible for glaciating the modeled clouds. The ice particles are primarily initiated by deposition-condensation nucleation prior to the formation of liquid water. In contrast, previous observations of polar maritime clouds suggested that glaciation was initiated by freezing of the larger cloud drops [Rangno and Hobbs, 1991]. Additionally, in-situ observations of Arctic mixed-phase stratus during the FIRE-ACE experiment show that vapor-grown crystals comprise only a small percentage of the total distribution of ice particles [Lawson et al., 2001; Rangno and Hobbs, 2001]. This difference between modeled and observed ice initiation mechanisms may have

serious implications on the partitioning of the cloud phases in the simulation.

6. Sensitivity Tests and Discussion

[36] As stated in section 5, the deposition of water vapor onto cloud ice (PRD) and snow (PREI) is primarily responsible for glaciating the modeled clouds. Thus the liquid cloud fraction is expected to be quite sensitive to changes in PRD and PREI. Several model parameters influence PRD and PREI directly (see equations (A5) and (A17)), or indirectly through other cloud ice and snow microphysical processes that in turn determine the cloud ice and snow mixing ratios.

[37] We test the sensitivity of the model to values of the collection efficiency for riming, E_{ws} , the size threshold for autoconversion of cloud ice to snow, D_{auto} , the mean mass-weighted snow terminal fall velocity, V_s , the cloud ice terminal fall velocity, V_i , and the intercept of the snow size distribution, N_{0s} . The ranges used in the sensitivity tests were chosen to encompass all reasonable values for a given parameter. Since the modeled liquid cloud fraction exhibits little sensitivity to these parameters, we only briefly discuss the results. The mean IWC, IWP, IWP_{n0} , and LWP_{n0} , however, are relatively more sensitive to changes in E_{ws} , D_{auto} , V_s , V_i , and N_{0s} . The total precipitation at the surface is insensitive to changes in these parameters, and instead appears to be primarily influenced by the large-scale forcing

Table 9. Mean Process Terms in the Supersaturation Budget During the 10 min Prior to the Onset of Condensation and After the Onset of Evaporation^a

	Advection	Radiative Transfer	Turbulent Diffusion	Microphysical Processes
Condensation	16.6969	3.9995	8.0207	-20.4936
Evaporation	15.6817	4.1308	8.5942	-34.0528

^aValues given in $10^{-6} \text{ g kg}^{-1} \text{ s}^{-1}$.

(Morrison and Pinto, submitted manuscript, 2002). While uncertainties associated with these microphysical parameters may explain some of the model bias, more detailed knowledge of Arctic ice microphysical properties is necessary in order to specify realistic values for the parameters.

[38] We focus in greater detail on the cloud ice number concentration, N_i . Several studies have highlighted the importance of N_i to the maintenance of mixed-phase Arctic stratus [Pinto, 1998; Harrington *et al.*, 1999; Jiang *et al.*, 2000]. N_i is parameterized in the model as a function of T and S_i following Meyers *et al.* [1992; hereafter M92], which includes contributions from deposition- condensation and contact nucleation (see equations (A2)–(A4)). The deposition- condensation nucleation parameterization was derived from continuous-flow diffusion-chamber experiments. The contact nucleation parameterization was derived from measurements of aerosol/membrane filter and droplet interactions. Uncertainties associated with M92 may be several orders of magnitude at various temperatures and supersaturations when compared to parcel simulations using theoretical ice nucleation rates (V. I. Khvorostyanov and J. A. Curry, Toward the unified theory of heterogeneous ice nucleation, part 2: Parcel model simulation, submitted to *Journal of Atmospheric Science*, 2002). In addition, processes such as aggregation [e.g., Mitchell, 1988] and multiplication [e.g., Hallett and Mossop, 1974] may result in values of N_i much different from those associated with pristine ice. Therefore, we test the sensitivity of the model to a wide range of values of N_i . Sensitivities of the modeled cloud properties to variations in N_i of 0.01 to 100 times the baseline M92 formulation of N_i are shown in Figure 6. Most notably, liquid cloud fraction is highly dependent upon the value of N_i . As N_i is decreased to $0.01 \times$ M92, the liquid cloud fraction increases to 42.5%. Mean LWP also increases as N_i is decreased, while the mean LWP_{n0} does not show a clear relationship with N_i . Mean IWP and IWP_{n0} exhibit comparatively less sensitivity; for example, the mean IWP changes by only 26% across the range of N_i tested. The improved simulations of liquid water with decreasing values of N_i are consistent with other modeling studies of mixed-phase Arctic stratus [Girard and Curry, 2001; Jiang *et al.*, 2000]. Evidence of low ice nuclei concentrations in Arctic mixed-phase stratus clouds was suggested by observations taken during the FIRE-ACE experiment [Rogers *et al.*, 2001].

[39] Further insight into the modeled values of N_i is gained by discussing the relative contributions of contact and deposition- condensation nucleation. Deposition and condensation-freezing are two distinct nucleation mechanisms, although it is not usually possible to measure their separate contributions [Meyers *et al.*, 1992]; thus they are combined into a single formulation in equation (A3). Theoretical calculations of deposition nucleation rates by Khvorostyanov and Curry [2000] suggest that this mechanism is limited at temperatures warmer than ~ 250 K. Therefore, the combined deposition- condensation nucleation mechanism is expected to be limited in conditions of water subsaturation at temperatures greater than 250 K, since condensation freezing primarily occurs in conditions exceeding water saturation [Meyers *et al.*, 1992]. Excessive deposition- condensation nucleation in the model is consistent with differences between the modeled and

observed glaciation mechanisms. We examine the role of deposition- condensation nucleation by conducting a sensitivity test with this mechanism turned off (contact nucleation is still active when the cloud liquid water content exceeds the threshold of 10^{-5} g m $^{-3}$). The results of this sensitivity test are compared with baseline and retrieved values in Table 10. Liquid cloud fraction is much larger in the sensitivity simulation than in the baseline simulation, while the LWP_{n0} decreases, so that the mean LWP is relatively unchanged. Similar to the sensitivity tests varying the cloud ice number concentration, the mean IWP and IWP_{n0} are affected very little. Without deposition- condensation nucleation, however, the ice cloud fraction is somewhat underpredicted, particularly for higher-level clouds (>3 km), which may indicate that deposition nucleation is important above 3 km, where temperatures are generally less than 250 K. In contrast to the simulation with no deposition- condensation nucleation, turning off contact nucleation in the model has little effect on the simulation. These results suggest that a better understanding of ice nucleation in the Arctic environment, particularly regarding deposition- condensation nucleation, is necessary in order to improve the model simulations.

[40] Thus far, we have focused largely on the model sensitivity associated with uncertainties in the microphysical parameters. Several other nonmicrophysical factors may exert a large influence on the simulated clouds, including but not limited to: the advective and dynamic forcing, the surface and boundary-layer turbulent fluxes, the exclusion of horizontal condensed water advection, feedbacks between the clouds and the radiative transfer, and the spatial resolution. While it is beyond the scope of this paper to discuss each of these points at length, we examine in greater detail issues associated with the spatial resolution and the approach to cloud scale separation.

[41] One of the most important aspects of cloud modeling is the multiplicity of scales associated with cloud microphysical and macrophysical properties [e.g., Curry and Herman, 1985]. Differences in horizontal scale between the modeled (60×60 km average) and retrieved (measured at a single location) cloud properties may directly account for some of the model bias. Although the observed clouds during this time period are predominately stratiform (with the exception of ice crystal plumes associated with leads), horizontal variability in the retrieved LWP (estimated using the temporal variability and an advective timescale) suggests that subgrid scale variability in the cloud field is still significant. This difference likely accounts for the much larger overall variability in the retrieved cloud properties. Time-averaging of the modeled and retrieved cloud properties reduces the importance of this difference in scale in the comparisons. However, variability in the cloud field is important in setting values for scale-dependent microphysical parameters (e.g., the autoconversion thresholds), which are supposed to represent local in-cloud values [Fowler *et al.*, 1996]. Ignoring this scale dependence may reflect back on the mean cloud properties due to nonlinearities in the microphysical process rates.

[42] As stated briefly in section 2, ARCSM distinguishes between two types of cloudiness based upon a separation of scale: resolvable-scale clouds predicted by the bulk microphysics parameterization, and convective

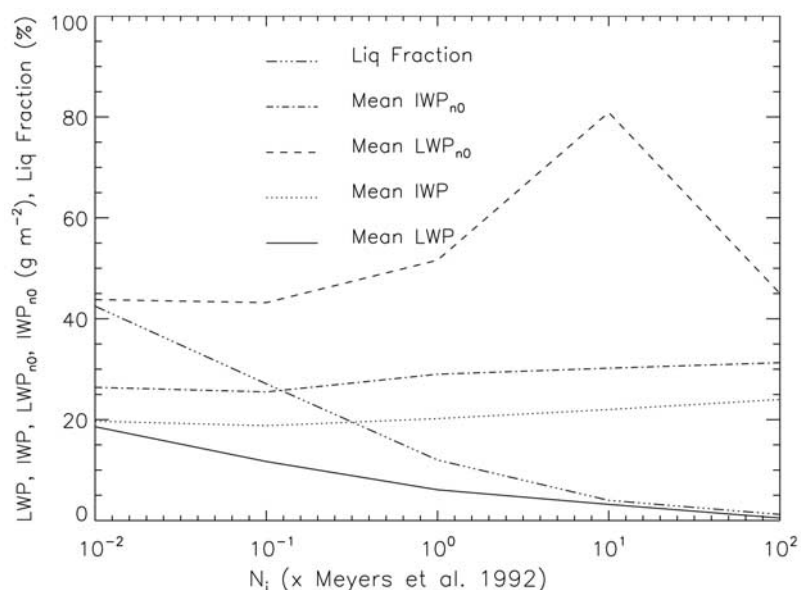


Figure 6. Sensitivities of modeled cloud properties to variations in the cloud ice number concentration. Specific cloud properties and units are indicated in the legend.

clouds predicted by the cumulus parameterization. This approach to scale separation follows that of several meso-scale models, including MM5 and ARCSyM, among others. While the grid-scale microphysics may resolve the largest convective elements of cloud systems depending upon the model resolution [Zhang *et al.*, 1988], due to the absence of deep convection at SHEBA, we assume that the resolved microphysics is entirely due to stratiform cloud processes. This approach to scale separation works quite well in simulating midlatitude cloud systems [e.g., Zhang *et al.*, 1988], however, the unique properties of Arctic clouds may necessitate a different type of subgrid parameterization. A critical assumption implicit in the present approach to scale separation is that stratiform cloud processes occur on a scale that is resolvable by ARCSyM, yet there is no physical explanation as to why this is necessarily true. Curry and Herman [1985] suggested that the seemingly anomalous occurrence of horizontally extensive stratiform cloud cover over the Beaufort Sea region in grid boxes (50 km horizontal resolution and 100 mb vertical resolution) with low average relative humidities was due to subgrid scale variability in the vertical. This feature resulted from the thin vertical extent of the clouds combined with a very sharp decrease in relative humidity above the cloud top. While the 100 mb vertical resolution used by the analysis of Curry and Herman [1985] is fairly coarse, observations suggest that the clouds at SHEBA are often subgrid at the resolution of ARCSyM as well (some liquid layers in mixed-phase clouds were observed to have thicknesses on the order of tens of meters). Increased variability in the vertical, relative to lower latitudes, may result from the strong static stability often encountered in the lower Arctic troposphere [Curry *et al.*, 1996], which inhibits mixing and leads to stratification of the atmospheric fields.

[43] An easy way to test the effects of subgrid scale vertical inhomogeneity is to increase the model resolution; however, in a SCM, where the thermodynamic properties

are strongly driven by the external forcing, the resolution of the forcing data must also be increased. High-resolution advective and dynamic forcing is not available at the present time; thus, the model's true sensitivity to changes in vertical resolution is difficult to test. Instead, we lower the liquid water condensation relative humidity threshold to determine an approximate value that is required to mimic the effects of subgrid variability in the saturation and correctly simulate the liquid cloud fraction (Figure 7). As expected, mean LWP and liquid cloud fraction increase substantially as the condensation threshold is decreased, while the mean IWP and IWP_{n0} exhibit comparatively little sensitivity. These results show that the large-scale condensation relative humidity threshold must be substantially lowered from saturation to approximately 88% in order to simulate the observed liquid cloud fraction. Further study is necessary to fully address this issue.

7. Conclusions

[44] In this study, a single column model (ARCSyM) coupled to the MM5mp cloud microphysics parameterization is evaluated using cloud properties retrieved at SHEBA during the period of 1 April to 16 May 1998. The study is

Table 10. Comparison of Simulated and Retrieved Water Paths and Cloud Fractions^{a,b}

	Mean LWP	Mean LWP _{n0}	Mean IWP	Mean IWP _{n0}	Liquid Cloud Fraction	Ice Cloud Fraction
Sensitivity	8.0	38.8	19.4	28.9	20.5	67.1
Baseline	6.1	51.6	20.2	26.5	12.0	76.0
Retrieved	25.6	36.2	34.6	41.1	64.4	74.8

^aValues of simulated and retrieved water paths are given in g m^{-2} , and values of cloud fractions are given in percent.

^b“Sensitivity” indicates the sensitivity test conducted with deposition nucleation turned off.

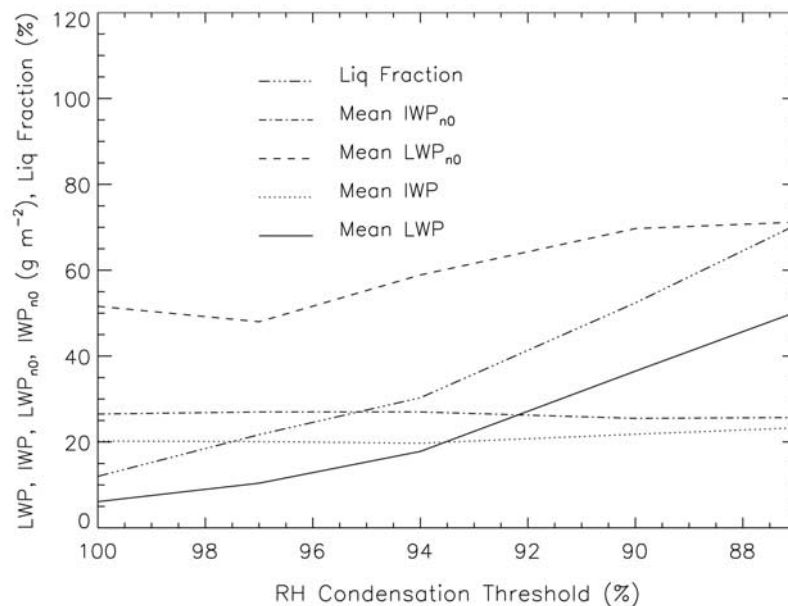


Figure 7. Sensitivities of modeled cloud properties to variations in the relative humidity condensation threshold. The baseline threshold relative humidity is 100%. Specific cloud properties and units are indicated in the legend.

broadly divided into two parts. First, we compare modeled and retrieved cloud properties. Second, we analyze the cloud liquid water and supersaturation budgets and conduct sensitivity tests to determine the relative importance of the various microphysical parameters to the model results. In addition, we discuss nonmicrophysical factors influencing the cloud properties.

[45] Overall, the model accurately simulates the cloud boundaries and total cloud fraction, but has difficulty correctly partitioning the cloud phases and predicting the condensed water contents and paths, particularly for low-level cloudiness. Difficulties in the analysis are associated with uncertainties in the advective forcing, differences in scale between the model and the retrievals, and uncertainties in the retrieval statistics, particularly for the ice phase. Key features of the comparison between the model and observations are:

[46] (1) Liquid cloud fraction is substantially underpredicted, leading to an underestimation of the mean LWP by 76%.

[47] (2) The mean in-cloud (mixed- and liquid-phase) liquid water path, LWP_{n0} , is overpredicted by 43%.

[48] (3) Ice cloud fraction and total cloud fraction are close to the observed values.

[49] (4) Mean IWP is underpredicted by 42%.

[50] (5) Most of the model bias is associated with lower-level cloudiness (<3 km). The upper-level (>3 km) mean IWP and IWC are close to the retrieved values.

[51] Underprediction of the mean LWP, resulting from the frequent representation of liquid- and mixed-phase clouds as entirely crystalline, is consistent with *Girard and Curry* [2001], using the MM5mp parameterization to model the 1–20 May period of SHEBA. Other models (SCM version of the CSU GCM [Fowler *et al.*, 1996] and ECMWF) underpredict the liquid cloud fraction and mean LWP in simulations of the May 1998 period of SHEBA as well [Curry *et al.*, 2000].

[52] Biases in the liquid cloud fraction, and, subsequently, the mean LWP, are discussed in the context of errors in the formation and dissipation of cloud liquid water events. An analysis of the cloud liquid water budget suggests that condensation/evaporation of cloud drops, PCC, is the primary term driving both the formation and dissipation of the cloud liquid water events. PCC is in turn determined by the absolute supersaturation, δM . The tendency of δM is dominated by the deposition of water vapor onto cloud ice and snow as a sink term during dissipation of the liquid water. Thus the Bergeron-Findeisen mechanism is primarily responsible for glaciating the modeled clouds; preferential depositional growth of ice over liquid results in a drying of the atmosphere and subsequent evaporation of the cloud drops. Cloud ice is primarily initiated by deposition-condensation nucleation prior to the formation of the liquid water. Direct freezing of cloud drops is of little importance. In contrast, previous observations of polar clouds suggested that glaciation was initiated by freezing of the larger cloud drops [Rangno and Hobbs, 1991]. This difference between modeled and observed ice initiation mechanisms may have serious implications on the partitioning of the cloud phases in the simulations.

[53] Sensitivity tests reveal that the liquid cloud fraction is influenced very little by changes in the collection efficiency for riming onto snow, the size threshold for auto-conversion of cloud ice to snow, the terminal fall velocities of cloud ice and snow, and the intercept of the snow size distribution. However, the mean IWP, IWP_{n0} , and LWP_{n0} are quite sensitive to changes in these parameters. The liquid cloud fraction exhibits a large sensitivity to the ice crystal number concentration, given the wide range of uncertainty associated with this parameter. Sensitivity tests suggest that, more specifically, uncertainties in the formulation of deposition-condensation nucleation may be associated with the bias in the liquid cloud fraction. Excessive deposition-condensation nucleation in the model is consis-

tent with differences between the modeled and observed glaciation mechanisms. These results suggest that a more detailed treatment of ice nucleation is necessary to adequately model mixed-phase Arctic stratus.

[54] We also discuss issues associated with the model resolution and the approach to cloud scale separation. The difference in scale between the model (60×60 km average) and observations (measured at a single location) likely accounts for the larger variability in the retrieved cloud properties, but is less important in comparing the mean cloud properties due to the time-averaging. However, the spatial scale of the model is important in determining appropriate values for resolution-dependent parameters in the microphysics scheme [Fowler *et al.*, 1996].

[55] The model's current approach to cloud scale separation, based on distinguishing between large-scale stratiform clouds predicted with the microphysics parameterization and small-scale convective clouds predicted with the cumulus parameterization, may not be appropriate over the Arctic multiyear ice zone where the stratiform clouds appear to be associated with inherently different spatial scales (particularly in the vertical) relative to lower latitudes. Testing the model's sensitivity to increasing resolution is difficult because there is no high-resolution advective forcing available at the present, so instead we lower the liquid water condensation threshold to mimic the effects of subgrid variability in the humidity. It is shown that the threshold relative humidity must be significantly reduced in order to correctly simulate the liquid cloud fraction. Further study is needed to fully understand the importance of subgrid variability in the cloud field in modeling Arctic clouds.

[56] In addition, several other factors that have not been addressed in this paper may have a large influence on the modeled cloud properties. In particular, uncertainties in the temperature and water vapor advective forcing and the exclusion of horizontal cloud water advection may lead to model deficiencies. Uncertainties in the ECMWF advective forcing and their influence on the model results are detailed by Morrison and Pinto (submitted manuscript, 2003).

[57] Low-level clouds in the Arctic typically form as a result of large-scale air mass modification [Curry, 1983]. Thus, movement and interaction of these air masses may be an additional source of condensed water through the horizontal advection of cloudiness. The relative importance of horizontal advection as a source of cloud water needs to be clarified in future work.

Appendix A: Formulations of the Microphysical Processes

[58] The microphysical scheme is a version of the Dudhia [1989] parameterization modified for use in MM5. Two additional modifications were made during the implementation into ARCSCM: the Fletcher [1962] formulation for ice crystal number concentration was replaced by Meyers *et al.* [1992], and an equation for the freezing of rain to form snow (NUFCIR) was added.

[59] The initiation (primary nucleation) of cloud ice (PRI) is given by [Dudhia, 1989]:

$$\text{PRI} = \max \left[\frac{M_0 N_i - q_i}{\Delta t}, 0 \right], \quad (\text{A1})$$

where $M_0 = 10^{-12}$ kg, Δt is the model time step, and the number concentration of ice nuclei, N_i (kg^{-1}), due to condensation-deposition ($N_{i,\text{dep}}$) and contact-freezing ($N_{i,\text{con}}$) nucleation is given by Meyers *et al.* [1992]:

$$N_i = N_{i,\text{dep}} + N_{i,\text{con}}, \quad (\text{A2})$$

where

$$N_{i,\text{dep}} = \frac{1000}{\rho} \exp(c_1 + c_2[100(S_i - 1)]) \quad \text{and} \quad (\text{A3})$$

$$N_{i,\text{con}} = \frac{1000}{\rho} \exp(c_3 + c_4[T_0 - T]). \quad (\text{A4})$$

The coefficients c_1 , c_2 , c_3 , and c_4 have values of -0.639 , 0.1296 , -2.8 , and 0.262 , respectively, T_0 is 273.15 K, and S_i is the saturation ratio with respect to ice. Contact nucleation is initiated only if cloud liquid water is present, indicated by a cloud liquid water content ($1000 \rho q_c$) greater than or equal to the cloud fraction threshold of 10^{-5} g m^{-3} (see section 2), and the temperature is less than 271.15 K. Following Meyers *et al.* [1992], deposition-condensation nucleation is prevented at temperatures warmer than 268.15 K. We note that the Meyers *et al.* [1992] parameterization is strictly applicable for temperatures between 253 K and 266 K and water supersaturations of -5% to 4.5% ; thus, some error may result from extrapolating to other environmental conditions.

[60] The deposition/sublimation of ice crystals (PRD) is given by a diffusional balance [Dudhia, 1989]:

$$\text{PRD} = \frac{4D_i(S_i - 1)\rho N_i}{A + B}, \quad (\text{A5})$$

where

$$A = \frac{L_s^2 \rho}{K_a R_v T^2}, \quad B = \frac{1}{q_{\text{vsi}} \xi}, \quad (\text{A6})$$

q_{vsi} is the water vapor mixing ratio at saturation with respect to ice, K_a is the thermal conductivity of air, R_v is the gas constant for water vapor, and ξ is the diffusivity of water vapor in air. The mean diameter of ice crystals, D_i , is found from the mean mass, $M_i = q_i/N_i$, using the mass-diameter relation for hexagonal plates from Rutledge and Hobbs [1983], $D_i = 16.3 M_i^{1/2}$.

[61] The heterogeneous freezing of cloud liquid water (NUFCI) is calculated following Bigg [1953]:

$$\text{NUFCI} = B'(\exp[A'(T_0 - T)] - 1) \frac{\rho q_c^2}{\rho_w N_c}, \quad (\text{A7})$$

where $A' = 0.66 \text{ K}^{-1}$, $B' = 100 \text{ m}^{-3} \text{ s}^{-1}$, T_0 is 273.15 K, ρ_w is the density of liquid water, and the number concentration of cloud drops, N_c , is assumed to be 10^8 m^{-3} .

[62] Homogeneous freezing of cloud liquid water (HOFCI) occurs instantaneously (i.e., within a model time step) at -40°C , while cloud ice instantaneously melts (MLTIC) at 0°C . These calculations are made after determining the other microphysical process rates (including fall velocity divergence), to ensure that there is no liquid water

in the model at temperatures below -40°C and no cloud ice at temperatures above 0°C . Snow, however, may persist at temperatures greater than 0°C .

[63] Terminal fall speeds for rain and snow are given by $V_f(D) = aD^b$, where D is the particle diameter. Values for a and b are given by *Locatelli and Hobbs* [1974]. For rain, $a = 841.99667 \text{ m}^{1/b} \text{ s}^{-1}$, and $b = 0.8$. For snow, $a = 11.72 \text{ m}^{1/b} \text{ s}^{-1}$, and $b = 0.41$ (values are for aggregates of unrimmed plates, planes, bullets, and columns). Cloud ice fall velocity is calculated following *Heymsfield and Donner* [1990]:

$$\bar{V} = 3.29(\rho q_i)^{0.16}. \quad (\text{A8})$$

[64] Marshall-Palmer size distributions are assumed for rain and snow, so that the size distribution function, $N(D)$, is given by:

$$N(D) = N_0 \exp(-\lambda D), \quad (\text{A9})$$

where N_0 is the intercept parameter, and λ is the slope:

$$\lambda = \left(\frac{\pi N_0 \rho_x}{\rho q_x} \right)^{\frac{1}{4}}. \quad (\text{A10})$$

Here q_x is the rain or snow mixing ratio, and ρ_x is the density (1000 kg m^{-3} for rain, 100 kg m^{-3} for snow). For rain, the intercept parameter is $N_0 = 8 \times 10^6 \text{ m}^{-4}$ [*Dudhia*, 1989]. For snow, N_0 varies as a function of the snow mixing ratio, following *Sekhon and Srivastava* [1970]:

$$N_0 = \left(1.05 \left[\frac{1}{\rho q_s \alpha} \left(\frac{\pi \rho_s}{\rho q_s} \right)^{\frac{b}{4}} \right]^{0.94} \right)^{\frac{4}{0.94b+4}}, \quad (\text{A11})$$

where

$$\alpha = \frac{a\Gamma(4+b)}{6\rho_s}, \quad (\text{A12})$$

ρ_s is the density of the snow particles, Γ is the Euler gamma function, and the values of the fall speed parameters a and b are those for snow.

[65] The mass-weighted mean terminal velocity for rain and snow is defined as:

$$\bar{V} = \frac{a\Gamma(4+b)}{6\lambda^b}, \quad (\text{A13})$$

with the appropriate values of λ , a , and b for rain or snow.

[66] Autoconversion of cloud liquid water to rain (PRC) is given by [*Kessler*, 1969]:

$$\text{PRC} = \max[k_1(q_c - q_{\text{crit}}), 0], \quad (\text{A14})$$

where $k_1 = 10^{-3} \text{ s}^{-1}$ and $q_{\text{crit}} = 0.5 \text{ g kg}^{-1}$.

[67] Autoconversion of cloud ice to snow (PRCI) is given by [*Lin et al.*, 1983]:

$$\text{PRCI} = \max\left[\frac{(q_i - M_{\text{max}}N_i)}{\Delta t}, 0 \right], \quad (\text{A15})$$

where $M_{\text{max}} = 9.4 \times 10^{-10} \text{ kg}$ and N_i is given by equation (A2). M_{max} corresponds to a size threshold of $500 \mu\text{m}$, given the mass-diameter relationship for hexagonal plates from *Rutledge and Hobbs* [1983].

[68] The accretion of cloud liquid by rain (PRA), cloud ice by snow (PRAI), and cloud liquid water by snow (PSACW) are given by [*Dudhia*, 1989]:

$$\text{PRA, PRAI, PSACW} = \frac{1}{4} \pi \rho a q_x E N_0 \frac{\Gamma(3+b)}{\lambda^{3+b}}, \quad (\text{A16})$$

where E is the collection efficiency ($E = 1$ for PRA, $E = 0.1$ for PRAI, and $E = 1$ for PSACW), N_0 , a , and b are the relevant values of the slope intercept and fall speed parameters for rain (PRA) or snow (PRAI, PSACW), q_x is the mixing ratio of cloud liquid water (PRA, PSACW) or cloud ice (PRAI), and λ is given by (A10), with the appropriate values for rain (PRA) or snow (PRAI, PSACW). Collisions between cloud ice/rain and snow/rain are neglected.

[69] The condensation/evaporation of rain (PRE) and deposition/sublimation of snow (PREI) are given by [*Rutledge and Hobbs*, 1983]:

$$\text{PRE, PREI} = \frac{2\pi N_0(S-1)}{\lambda^2(A+B)} \left[f_1 + f_2 \left(\frac{a\rho}{\mu} \right)^{\frac{1}{2}} S_c^{\frac{1}{2}} \frac{\Gamma(\frac{5}{2} + \frac{b}{2})}{\lambda^{\frac{1}{2} + \frac{b}{2}}} \right], \quad (\text{A17})$$

with the relevant values of N_0 , a , and b chosen for rain or snow, and S is the saturation ratio with respect to liquid or ice. λ is given by equation (A10), with the appropriate values for rain or snow. The definitions of A and B change for rain, substituting L_v for L_s and q_{vs} for q_{vsi} in equation (A6). For snow, 2π is replaced by 4 . The bracketed term represents a ventilation factor, with the values of f_1 and f_2 given by 0.78 and 0.32 for rain and 0.65 and 0.44 for snow. The Schmidt number is given by $S_c = \mu/\rho\xi$, where μ is the viscosity of air.

[70] Melting of snow to form rain (PSMLT) is given by [*Rutledge and Hobbs*, 1983]:

$$\text{PSMLT} = \frac{2\pi N_0 K_a (T - T_0)}{\lambda^2 L_f} \left[f_1 + f_2 \left(\frac{a\rho}{\mu} \right)^{\frac{1}{2}} S_c^{\frac{1}{2}} \frac{\Gamma(\frac{5}{2} + \frac{b}{2})}{\lambda^{\frac{1}{2} + \frac{b}{2}}} \right], \quad (\text{A18})$$

where N_0 is given by equation (A11) and λ is given by equation (A10) with the appropriate values for snow.

[71] Freezing of rain to form snow (NUFCIR) follows from *Bigg* [1953]:

$$\text{NUFCIR} = 20\pi^2 B' N_0 \frac{\rho_w}{\rho} (\exp[A'(T_0 - T)] - 1) \lambda^{-7}, \quad (\text{A19})$$

where values of A , and B , are those used in equation (A7), N_0 is that for rain, and λ is given by equation (A10) with the appropriate values for rain.

[72] Cloud liquid water condensation/evaporation (PCC) is calculated after determining the other microphysical process rates (with the exception of fall velocity divergence and HOFCI/MLTIC) [*Dudhia*, 1989]. First, temperature, cloud water mixing ratio, and water vapor mixing ratio are forecast at the advanced model time step, designated as

T' , q'_c , q'_v , respectively. If $\delta M = q'_v - q'_{vs} > 0$, where q'_{vs} is the saturation mixing ratio at T' , then PCC is given by (condensation):

$$\text{PCC} = \frac{r_1 \delta M}{\Delta t}, \quad (\text{A20})$$

where r_1 is the psychrometric correction associated with the latent heat of condensation:

$$r_1 = \frac{1}{1 + \frac{L_v^2 q'_{vs}}{R_v c_p T^2}}. \quad (\text{A21})$$

[73] If $\delta M < 0$, then PCC is given by (evaporation):

$$\text{PCC} = -\min\left(-\frac{r_1 \delta M}{\Delta t}, \frac{q'_c}{\Delta t}\right). \quad (\text{A22})$$

[74] The fall terms in equations (4)–(6) are calculated at the advanced time step after calculating the microphysical process rates and updating the prognostic condensed water variables. Fall terms are calculated on split time steps to ensure numerical stability. Because of the finite model time step, process rates may occasionally become large enough that the water species can become negative. To conserve the water mass, the individual process rates are divided by the sum of the rates in this instance.

Notation

a	Constant in fallspeed-diameter relationship	k_1	Autoconversion rate of cloud water to rain
a_1	Constant in IWC-reflectivity relationship	K_a	Thermal conductivity of air
A	Thermodynamic term in condensation/deposition	LWP	Liquid water path
A'	Constant in heterogeneous freezing formula	LWP_{n0}	Mean in-cloud (mixed- and liquid- phase) liquid water path
ADV	Time-averaged vertically-integrated 3-D water vapor advection	L_f	Latent heat of fusion
b	Constant in fallspeed-diameter relationship	L_v	Latent heat of vaporization
b_1	Constant in IWC-reflectivity relationship	L_s	Latent heat of sublimation
B	Thermodynamic term in condensation/deposition	M_0	Mass of newly initiated ice crystal
B'	Constant in heterogeneous freezing formula	MF	Mean mass flux of water vapor at the surface
c_1	Constant in cloud ice number concentration formula	M_i	Mean mass of ice crystal
c_2	Constant in cloud ice number concentration formula	N	Size distribution function
c_3	Constant in cloud ice number concentration formula	N_0	Slope intercept in Marshall-Palmer distribution
c_4	Constant in cloud ice number concentration formula	N_c	Cloud droplet number concentration
D	Particle diameter	N_i	Cloud ice number concentration
D_{auto}	Size threshold for autoconversion of cloud ice to snow	$N_{i,\text{con}}$	Cloud ice number concentration from contact nucleation
D_i	Mean diameter of cloud ice	$N_{i,\text{dep}}$	Cloud ice number conc. from dep. and cond. nucleation
E	Collection efficiency	p	Air pressure
E_{ws}	Collection efficiency for riming of liquid water	PREC	Total liquid-equivalent precipitation at the surface
f_1	Constant in ventilation factor calculation	p_s	Surface air pressure
f_2	Constant in ventilation factor calculation	p_{top}	Air pressure at the top of the model
g	Gravitational acceleration	PWV	Precipitable water vapor
IWC	Ice water content	q_c	Cloud liquid water mixing ratio
IWP	Ice water path	q_{crit}	Threshold for autoconversion of cloud liquid water to rain
IWP_{n0}	Mean in-cloud (mixed- and ice- phase) ice water path	q_i	Cloud ice mixing ratio
		q_r	Rain mixing ratio
		q_s	Snow mixing ratio
		q_v	Water vapor mixing ratio
		q_{vs}	Water vapor mixing ratio at saturation with respect to liquid
		q_{vsi}	Water vapor mixing ratio at saturation with respect to ice
		q_x	Mixing ratio of arbitrary species
		r_1	Correction factor in condensational growth
		R_d	Gas constant for dry air
		R_v	Gas constant for water vapor
		S	Saturation ratio
		S_c	Schmidt number
		S_i	Saturation ratio with respect to ice
		S_w	Saturation ratio with respect to liquid water
		t	Time
		T	Temperature
		T_0	Temperature at freezing point
		\vec{v}	Horizontal wind vector
		V_f	Terminal fall velocity
		\bar{V}	Mass-weighted mean terminal velocity
		Z	Reflectivity
		δM	Absolute supersaturation at advanced time step
		δ_c	Turbulent flux divergence of cloud liquid water
		δ_i	Turbulent flux divergence of cloud ice
		δt	Length of simulation time period
		Δt	Model time step
		Γ	Euler gamma function
		λ	Slope parameter in size distribution
		ρ	Density of air
		ρ_s	Density of snow
		ρ_w	Density of liquid water
		ρ_x	Density of arbitrary hydrometeor species
		μ	Viscosity of air

- σ Model sigma level
 ω Vertical pressure velocity
 ξ Diffusivity of water vapor in air

[75] **Acknowledgments.** This research was supported by DOE ARM grant DE-FG03-94ER61771 and NSF SHEBA grant OPP-0084225. Contributions by M. Shupe were supported by NASA FIRE-ACE contract L642050 and NSF SHEBA agreement OPP-9701730. Microwave radiometer data were obtained from ARM. Precipitation gauge and rawinsonde measurements were obtained from the SHEBA Project Office at the University of Washington Applied Physics Laboratory. Surface forcing data were obtained from the SHEBA Atmospheric Surface Flux Group. We are grateful to C. Jakob and his colleagues at the ECMWF for providing the model dynamical forcing. Special thanks to T. Uttal, who facilitated the collection and analysis of the radar data. The comments of three anonymous reviewers greatly improved the manuscript.

References

- Bigg, E. K., The supercooling of water, *Proc. Phys. Soc. London, Sect. B*, *66*, 688–694, 1953.
- Briegleb, B. P., Delta-eddington approximation for solar radiation in the NCAR Community Climate Model, *J. Geophys. Res.*, *97*, 7603–7612, 1992.
- Considine, G., J. A. Curry, and B. Wielicki, Modeling cloud fraction and horizontal variability in marine boundary layer clouds, *J. Geophys. Res.*, *102*, 13,517–13,525, 1997.
- Curry, J. A., On the formation of polar continental air, *J. Atmos. Sci.*, *40*, 2279–2292, 1983.
- Curry, J. A., Interactions among turbulence, radiation, and microphysics in Arctic stratus clouds, *J. Atmos. Sci.*, *43*, 90–106, 1986.
- Curry, J. A., and E. E. Ebert, Sensitivity of the thickness of Arctic sea ice to the optical properties of clouds, *Ann. Glaciol.*, *14*, 43–46, 1990.
- Curry, J. A., and G. F. Herman, Relationships between large-scale heat and moisture budgets and the occurrence of Arctic stratus clouds, *Mon. Weather Rev.*, *113*, 1441–1457, 1985.
- Curry, J. A., E. E. Ebert, and J. L. Schramm, Impact of clouds on the surface radiation balance of the Arctic Ocean, *Meteorol. Atmos. Phys.*, *51*, 197–217, 1993.
- Curry, J. A., W. B. Rossow, D. Randall, and J. L. Schramm, Overview of Arctic cloud and radiation properties, *J. Clim.*, *9*, 1731–1764, 1996.
- Curry, J. A., et al., FIRE Arctic Clouds Experiment, *Bull. Am. Meteorol. Soc.*, *81*, 5–29, 2000.
- Dudhia, J., Numerical study of convection observed during the Winter Monsoon Experiment using a mesoscale two-dimensional model, *J. Atmos. Sci.*, *46*, 3077–3107, 1989.
- Ebert, E. E., and J. A. Curry, A parameterization of ice-cloud optical properties for climate models, *J. Geophys. Res.*, *97*, 3831–3836, 1992.
- Fletcher, N. H., *The Physics of Rainclouds*, 386 pp., Cambridge Univ. Press, New York, 1962.
- Fowler, L. D., D. A. Randall, and S. A. Rutledge, Liquid and ice microphysics in the CSU General Circulation Model, part I: Model description and simulated microphysical processes, *J. Clim.*, *9*, 489–529, 1996.
- Girard, E., and J. A. Curry, Simulation of Arctic low-level clouds observed during the FIRE Arctic Clouds Experiment using a new bulk microphysics scheme, *J. Geophys. Res.*, *106*, 15,139–15,154, 2001.
- Grell, G. A., Prognostic evaluation of assumptions used by cumulus parameterizations, *Mon. Weather Rev.*, *121*, 764–787, 1993.
- Gunn, K. L. S., and J. S. Marshall, The distribution with size of aggregate snowflakes, *J. Meteorol.*, *15*, 452–461, 1958.
- Hallett, J., and S. C. Mossop, Production of secondary ice particles during the riming process, *Nature*, *249*, 26–28, 1974.
- Harrington, J. Y., T. Reisin, W. R. Cotton, and S. M. Kreidenweis, Cloud resolving simulations of Arctic stratus, part II: Transition-season clouds, *Atmos. Res.*, *51*, 45–75, 1999.
- Heymsfield, A. J., and L. J. Donner, A scheme for parameterizing ice-cloud water content in general circulation models, *J. Atmos. Sci.*, *47*, 1865–1877, 1990.
- Holtzlag, A. M., and B. A. Boville, Local versus non-local boundary-layer diffusion in a global climate model, *J. Clim.*, *6*, 1825–1842, 1993.
- Intrieri, J. M., M. D. Shupe, T. Uttal, and B. J. McCarty, Annual cycle of Arctic cloud geometry and phase from radar and lidar at SHEBA, *J. Geophys. Res.*, *107*(C10), 8030, doi:10.1029/2000JC000423, 2002.
- Jiang, H., W. R. Cotton, J. O. Pinto, J. A. Curry, and M. J. Weisbluth, Cloud resolving simulations of mixed-phase Arctic stratus observed during BASE: Sensitivity to concentration of ice crystals and large-scale heat and moisture advection, *J. Atmos. Sci.*, *57*, 2105–2117, 2000.
- Kessler, E., On the distribution and continuity of water substance in atmospheric circulations, *Meteorol. Monogr.*, *10*, 84 pp., 1969.
- Khvorostyanov, V. I., and J. A. Curry, Toward the theory of stochastic condensation in clouds, part I: A general kinetic equation, *J. Atmos. Sci.*, *56*, 3985–3996, 1999.
- Khvorostyanov, V. I., and J. A. Curry, A new theory of heterogeneous ice nucleation for application in cloud and climate models, *Geophys. Res. Lett.*, *27*, 4081–4084, 2000.
- Lawson, R. P., B. A. Baker, C. G. Schmitt, and T. L. Jensen, An overview of microphysical properties of Arctic clouds observed in May and July 1998 during FIRE ACE, *J. Geophys. Res.*, *106*, 14,989–15,014, 2001.
- Lin, Y.-L., R. D. Farley, and H. D. Orville, Bulk parameterization of the snow field in a cloud model, *J. Clim. Appl. Meteorol.*, *22*, 1065–1092, 1983.
- Locatelli, J. D., and P. V. Hobbs, Fallspeeds and masses of solid precipitation particles, *J. Geophys. Res.*, *79*, 2185–2197, 1974.
- Lynch, A. H., W. L. Chapman, J. E. Walsh, and G. Weller, Development of a regional climate model of the western Arctic, *J. Clim.*, *8*, 1555–1570, 1995.
- Matrosov, S. Y., Retrievals of vertical profiles of ice cloud microphysics from radar and IR measurements using tuned regressions between reflectivity and cloud parameters, *J. Geophys. Res.*, *104*, 16,741–16,753, 1999.
- Matrosov, S. Y., A. V. Korolev, and A. J. Heymsfield, Profiling cloud ice mass and particle characteristic size from Doppler radar measurements, *J. Atmos. Oceanic Technol.*, *19*, 1003–1018, 2002.
- Meyers, M. P., P. J. Demott, and W. R. Cotton, New primary ice nucleation parameterization in an explicit model, *J. Appl. Meteorol.*, *31*, 708–721, 1992.
- Mitchell, D. L., Evolution of snow-size spectra in cyclonic storms, part I: Snow growth by vapor deposition and aggregation, *J. Atmos. Sci.*, *45*, 3431–3451, 1988.
- Mlawer, E. J., S. J. Taubman, P. D. Brown, M. J. Iacono, and S. A. Clough, Radiative transfer for inhomogeneous atmospheres: RRTM a validated correlated-k model for the longwave, *J. Geophys. Res.*, *102*, 16,663–16,682, 1997.
- Ose, T., An examination of the effects of explicit cloud water in the UCLA GCM, *J. Meteorol. Soc. Jpn.*, *71*, 93–109, 1993.
- Persson, P. O. G., C. W. Fairall, E. L. Andreas, P. S. Guest, and D. K. Perovich, Measurements near the Atmospheric Surface Flux Group tower at SHEBA: Near-surface conditions and surface energy budget, *J. Geophys. Res.*, *107*(C10), 8045, doi:10.1029/2000JC000705, 2002.
- Pinto, J. O., Autumnal mixed-phase cloudy boundary layers in the Arctic, *J. Atmos. Sci.*, *55*, 2016–2038, 1998.
- Randall, D. A., and D. G. Cripe, Alternative methods for specification of observed forcing in single-column models and cloud system models, *J. Geophys. Res.*, *104*, 24,527–24,545, 1999.
- Randall, D. A., K. M. Xu, R. J. Somerville, and S. Iacobellis, Single-column models and cloud ensemble models as links between observations and climate models, *J. Clim.*, *9*, 1683–1697, 1996.
- Rangno, A. L., and P. V. Hobbs, Ice particle and precipitation development in small polar maritime cumulus clouds, *Q. J. R. Meteorol. Soc.*, *117*, 207–241, 1991.
- Rangno, A. L., and P. V. Hobbs, Ice particles in stratiform clouds in the Arctic and possible mechanisms for the production of high ice concentrations, *J. Geophys. Res.*, *106*, 15,065–15,075, 2001.
- Rogers, D. C., P. J. DeMott, and S. M. Kreidenweis, Airborne measurements of tropospheric ice-nucleating aerosol particles in the Arctic spring, *J. Geophys. Res.*, *106*, 15,053–15,063, 2001.
- Rutledge, S. A., and P. V. Hobbs, The mesoscale and microscale structure and organization of clouds and precipitation in mid-latitude cyclones, Part VIII: A model for the “seeder-feeder” process in warm-frontal rainbands, *J. Atmos. Sci.*, *40*, 1185–1206, 1983.
- Schramm, J. L., M. M. Holland, J. A. Curry, and E. E. Ebert, Modeling the thermodynamics of a sea ice thickness distribution. 1: Sensitivity to ice thickness resolution, *J. Geophys. Res.*, *102*, 23,079–23,091, 1997.
- Sekhon, R. S., and R. C. Srivastava, Snow spectra and radar reflectivity, *J. Atmos. Sci.*, *27*, 299–307, 1970.
- Shupe, M. D., T. Uttal, S. Y. Matrosov, and A. S. Frisch, Cloud water contents and hydrometeor sizes during the FIRE Arctic Clouds Experiment, *J. Geophys. Res.*, *106*, 15,015–15,028, 2001.
- Slingo, A., A GCM parameterization for the shortwave optical properties of water clouds, *J. Atmos. Sci.*, *46*, 1419–1427, 1989.
- Stokes, G. M., and S. E. Schwartz, The Atmospheric Radiation Measurement (ARM) Program: Programmatic background and design of the

- cloud and radiation test bed, *Bull. Am. Meteorol. Soc.*, 75, 1201–1221, 1994.
- Uttal, T., et al., The Surface Heat Budget of the Arctic Ocean, *Bull. Am. Meteorol. Soc.*, 83, 255–275, 2002.
- Westwater, E. R., Y. Han, M. D. Shupe, and S. Y. Matrosov, Analysis of integrated cloud liquid and precipitable water vapor retrievals from microwave radiometers during SHEBA, *J. Geophys. Res.*, 106, 32,019–32,030, 2001.
- Zhang, D.-L., E.-Y. Hsie, and M. W. Moncrieff, A comparison of explicit and implicit predictions of convective and stratiform precipitating weather systems with a meso-b-scale numerical model, *Q. J. R. Meteorol. Soc.*, 114, 31–60, 1988.
-
- J. A. Curry, School of Earth and Atmospheric Sciences, Georgia Institute of Technology, Atlanta, GA 30332-0340, USA. (curryja@eas.gatech.edu)
- H. Morrison, Program in Atmospheric and Oceanic Sciences, University of Colorado, Boulder, CO 80309, USA. (hugh@monsoon.colorado.edu)
- M. D. Shupe, NOAA Environmental Technology Laboratory, Boulder, CO 80303, USA. (matthew.shupe@noaa.gov)